J. Fluid Mech. (1981), *vol.* **109**, *pp.* 465-482
Printed in Great Britain

A numerical study of the deformation and burst of a viscous drop in general shear flows

By J. M. RALLISON

Department of Applied Mathematics and Theoretical Physics,
University of Cambridge,
Silver Street, Cambridge CB3 9EW

(Received 23 October 1980)

The time-dependent deformation and burst of a viscous drop in an arbitrary shear flow at zero Reynolds number is studied. The viscosities of the drop and the suspending fluid are assumed to be equal. A numerical scheme to track the (non-axisymmetric) drop shape in time is presented, and used to investigate the deformation induced by two-dimensional shear and orthogonal rheometer flows. Steady deformations, critical flow rates and burst modes are determined, and compared with asymptotic (small and large) deformation theories, and with experiment.

1. Introduction

The dynamics of an isolated small drop of fluid of viscosity $\lambda\mu$ freely suspended in a second fluid of viscosity μ which is caused to move in a prescribed manner have been the subject of several investigations, starting with the pioneering work of Taylor (1934). At vanishingly small Reynolds number the drop is able to translate with the same velocity as the local applied flow, but, in consequence of surface tension and the unequal viscosities, can neither freely deform in the local shear nor in general remain spherical. In a steady shear flow, a balance between viscous deforming stresses and the restoring forces generated by surface tension can give rise to a steady non-spherical drop shape, but, if the viscous forces are too strong, then the drop will break into two or more fragments.

The problems of determining the drop deformation and critical flow rate for burst have been tackled by several complementary techniques. Experimentally, the phenomena have been measured (in particular by Taylor 1934, and by Rumscheidt & Mason 1961) though the shear flows considered have been restricted in most investigations to either simple shear in a Couette device, or plane hyperbolic flow generated in a four-roller apparatus. Theoretically, there have been three main lines of attack. First, *small* drop deformations away from sphericity have been considered by several authors (a critical review has been given recently by Rallison 1980). These theories have provided good agreement with experiment for both weak flows for all values of λ, and for the entire range of flow strengths (provided the vorticity is non-zero) for large λ ($\gtrsim 5$). Second, *large* drop deformations have been examined by the methods of slender-body theory (Taylor 1964; Acrivos & Lo 1978; Hinch & Acrivos 1979, 1980). Such results are appropriate and quantitatively accurate for small values of λ ($\lesssim 0{\cdot}1$). Third, Rallison & Acrivos (1978; hereinafter referred to as I) have developed a numerical scheme which in principle covers the entire range of λ, but is, of course,

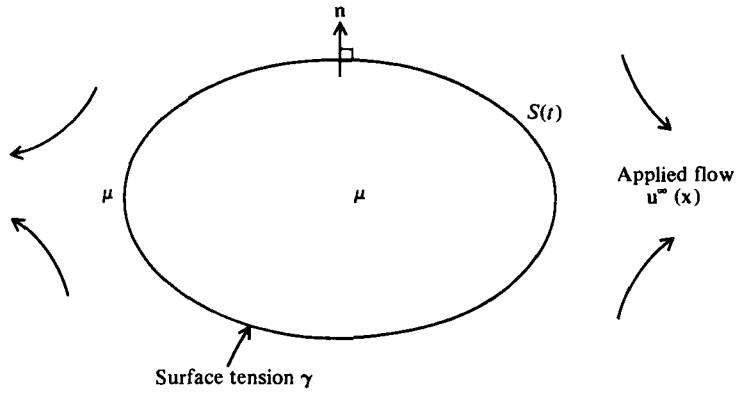

FIGURE 1. Definition sketch for the drop.

most useful for the intermediate ranges of λ and flow strength where the asymptotic theories do not apply.

In I, this scheme was used to analyse the time-dependent deformation of a drop for arbitrary (non-zero) λ in a uniaxial extensional flow. The important simplifying feature of such a flow is its axisymmetry, which gives rise to an axisymmetric (and so one-dimensional) deformed drop surface. The principal aim of the present paper is to treat general shear flows (such as simple shear and plane hyperbolic for which experimental data exist) so that the restriction to axisymmetry must be relaxed, thereby greatly increasing the computational complexity. We make instead the assumption that the viscosities of the discrete and continuous phases are the same ($\lambda = 1$): the numerical matrix inversion described in I is then unnecessary and the computation time is again reduced. The case appears experimentally typical of the intermediate λ range; there seems no reason to suppose that it is special except insofar as it provides a considerable mathematical simplification (given in § 2).

In § 3 the numerical scheme is presented, and the non-trivial problem of determining numerically the surface normals and curvatures is discussed. The principal results from asymptotic theories are collected in § 4 for comparison with the numerical results of § 5. Two-dimensional shear flows are investigated in detail in § 5 and equilibrium drop shapes, critical flow rates and burst modes are described. For these flows comparisons are also made with experiment. We finally consider briefly steady orthogonal rheometer flows, which are also experimentally feasible and have been used by Hakimi & Schowalter (1980) to study low-viscosity drops ($\lambda \approx 0{\cdot}1$). Unfortunately, no data have yet been reported in orthogonal rheometer flows for the $\lambda = 1$ drops considered here.

2. Formulation of the problem

As noted in I, the analysis of the deformation of a drop suspended in another fluid of the same viscosity ($\lambda = 1$) has the special simplifying feature that, as regards the equations which define the fluid velocity $\mathbf{u}$ at each instant of time, the *same* fluid may be regarded as occupying all space, but with a membrane of stokeslets provided by surface tension forces at the position of the interface S (see figure 1). These stokeslets have a strength proportional to the surface curvature $\nabla^S \mathbf{n}$ (where ∇^S is a two-dimen-

sional surface gradient) and to the surface tension coefficient γ, and hence generate a fluid velocity at an arbitrary point $\mathbf{x}$ given by

$$\mathbf{u}(\mathbf{x}) = -\frac{\gamma}{8\pi\mu}\int_S \mathbf{J}(\mathbf{x}-\mathbf{y}).\mathbf{n}\,\nabla^S\mathbf{n}\,dS_y,$$

where

$$\mathbf{J}(\mathbf{r}) = \mathbf{I}/r + \mathbf{rr}/r^3$$

is the Oseen tensor giving the fluid velocity at $\mathbf{r}$ produced by a point force at the origin in *unbounded* fluid. In view of the linearity of the Stokes equations, when the drop is placed in an applied flow $\mathbf{u}^\infty(\mathbf{x})$ the total fluid velocity is given simply by

$$\mathbf{u}(\mathbf{x}) = \mathbf{u}^\infty(\mathbf{x}) - \frac{\gamma}{8\pi\mu}\int_S \mathbf{J}(\mathbf{x}-\mathbf{y}).\mathbf{n}\,\nabla^S\mathbf{n}\,dS_y.$$

Now, in view of the supposed smallness of the drop, the applied flow $\mathbf{u}^\infty$ may be considered to vary linearly with position, so that

$$\mathbf{u}^\infty(\mathbf{x}) = G\boldsymbol{\Gamma}.\mathbf{x} = G(\mathbf{e}+\boldsymbol{\omega}).\mathbf{x},$$

where G is the shear rate, and $\mathbf{e}$, $\boldsymbol{\omega}$ are respectively the non-dimensional rate of strain and vorticity tensors. If the drop volume is $\frac{4}{3}\pi a^3$, then, scaling time by the surface tension time $4\pi\mu a/\gamma$ as in I, the deformation is governed by the non-dimensional parameter

$$\Omega = 4\pi\mu G a/\gamma$$

and the instantaneous velocity is given by

$$\mathbf{u}(\mathbf{x}) = \Omega(\mathbf{e}+\boldsymbol{\omega}).\mathbf{x} - \frac{1}{2}\int_S \mathbf{J}(\mathbf{x}-\mathbf{y}).\mathbf{n}\,\nabla^S\mathbf{n}\,dS_y. \tag{1}$$

In particular, this result is valid for points $\mathbf{x}$ which lie in S.

Now, with a given shear rate $\boldsymbol{\Gamma}(t)$ the deformation of the surface $S(t)$ from some prescribed initial shape $S(0)$ may be followed in time by the same technique as used in I: if $S(t)$ is known, the velocity $\mathbf{u}$ at each point $\mathbf{x}\in S(t)$ may be determined from (1), and hence x can be advanced to $\mathbf{x}+\Delta t\mathbf{u}.\mathbf{nn}$, and thus $S(t+\Delta t)$ is determined. This process may be repeated until S either attains a steady shape, or deforms without bound, or attempts to split into two or more components.

3. The numerical scheme

In using the approach outlined above it is necessary to approximate the surface $S(t)$ by means of a number of collocation points $\mathbf{x}_i, i = 1, \ldots, N$. Even if these are initially evenly spaced over $S(0)$, as the deformation proceeds they will become unevenly distributed, and so we devise first a numerical method to determine the surface normal and curvature at each point, and second a convenient scheme for evaluating the (singular) integral in (1).

3.1. *Determination of surface gradients and curvature*

Whereas in the corresponding two-dimensional (say axisymmetric) problem with $\mathbf{x}_i \in \mathscr{R}^2$ evaluation of surface tangents and curvatures is rendered a fairly straightforward matter by use of central differences even when the points are unevenly spaced, determining the surface curvature in the three-dimensional case is a non-trivial problem, principally because there is no simple analogous procedure.

In order to find the surface normal $\mathbf{n}_i$ and curvature κ_i at $\mathbf{x}_i$ we use the following method. In some neighbourhood $\mathscr{N}$ of $S(t)$ (specifically, within the smaller principal radius of curvature of the surface), let

$$f(\mathbf{x}) = \{\text{algebraic distance of } \mathbf{x} \text{ from } S(t)\} = \pm \inf\{|\mathbf{y}-\mathbf{x}| : \mathbf{y} \in S(t)\}$$

with the + or − sign chosen according as $\mathbf{x}$ is outside or inside S. Then $S(t)$ is given by

$$f(\mathbf{x}) = 0,$$

and f is infinitely differentiable in $\mathscr{N}$. Further, by construction

$$|\nabla f| = 1 \quad \text{for all} \quad \mathbf{x} \in \mathscr{N}$$

and hence

$$\mathbf{n}_i = \nabla f, \quad \kappa_i = \nabla^2 f.$$

We therefore require a numerical procedure to determine the first and second gradients of f at $\mathbf{x}_i \in S(t)$. Suppose then that $\mathbf{x}_j \in S(t)$ and let

$$\mathbf{h} = \mathbf{x}_j - \mathbf{x}_i.$$

Then

$$0 = f(\mathbf{x}_j) = f(\mathbf{x}_i) + \mathbf{h}.\nabla f(\mathbf{x}_i) + \tfrac{1}{2}\mathbf{hh}:\nabla\nabla f(\mathbf{x}_i) + O(h^3)$$
$$\to 0 + \mathbf{h}.\mathbf{n}_i + \tfrac{1}{2}\mathbf{hh}:\boldsymbol{\kappa}_i \quad \text{as} \quad |\mathbf{h}| \to 0,$$

where $\boldsymbol{\kappa}_i = \nabla\nabla f(\mathbf{x}_i)$ so that $\kappa_i = \operatorname{tr}\boldsymbol{\kappa}_i$. Now $\boldsymbol{\kappa}_i$ is a symmetric tensor, and thus we have nine unknowns $(\mathbf{n}_i, \boldsymbol{\kappa}_i)$ to be determined. We have at our disposal the equations

$$\mathbf{n}_i.\mathbf{n}_i = 1, \tag{2}$$

$$\nabla f.\nabla\nabla f = 0 \quad \text{so that} \quad \boldsymbol{\kappa}_i.\mathbf{n}_i = 0 \tag{3}_{1,2,3}$$

and, for any surface displacement $\mathbf{h}$,

$$\mathbf{n}_i.\mathbf{h} + \tfrac{1}{2}\mathbf{hh}:\boldsymbol{\kappa}_i = 0. \tag{4}$$

The last relation must therefore provide five independent (linear) equations for the unknowns, and thus for each point $\boldsymbol{\kappa}_i$ we require a list of five adjacent points for use in (4). We then have nine nonlinear algebraic equations (2), $(3)_{1,2,3}$, $(4)_{1,\ldots,5}$ for $(\mathbf{n}_i, \boldsymbol{\kappa}_i)$ which may be solved by an iterative Newton–Raphson procedure.

Two economies may be practised in evaluating $\mathbf{n}_i, \boldsymbol{\kappa}_i$ at each time t. First, since the change in each time step is slight, the values at the preceding time provide a good first estimate in the iteration. Second, since the majority of time in the Newton–Raphson routine is spent in setting up and inverting the 9×9 gradient matrix for the unknowns, and since this matrix changes little during the subsequent iteration, it is generally sufficient to compute the inverse just once for each point at each time step, and to use this *approximate* inverse to operate on the residuals. This saving in computation time greatly outweighs that lost in the occasional additional iteration required.

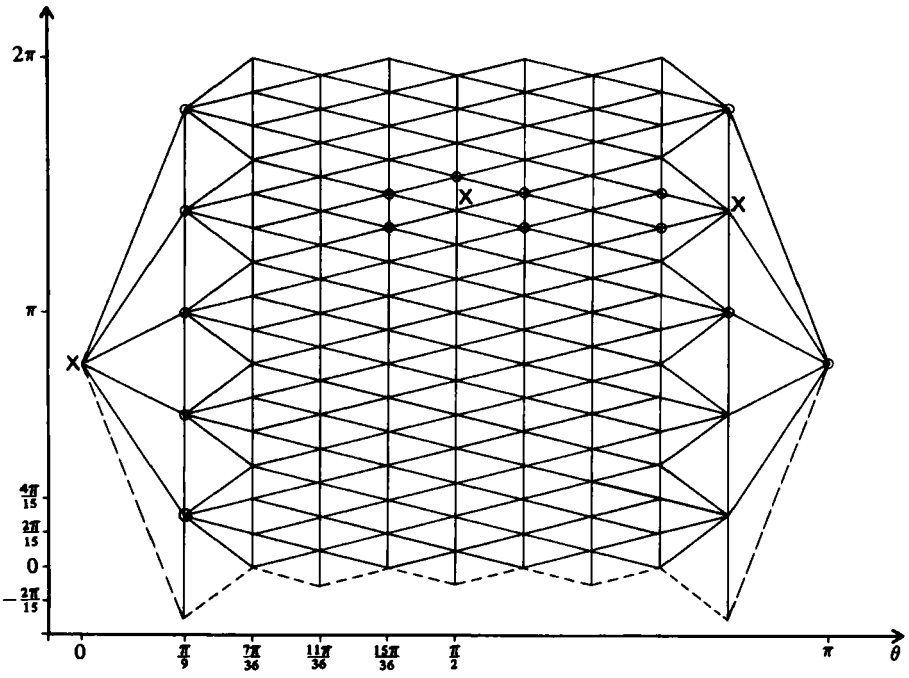

FIGURE 2. Choice of collocation points over a sphere in spherical polar co-ordinates.

3.2. *Evaluation of the surface integral*

We need also a convenient finite-difference representation of the integral in (1) where S is specified by unevenly distributed points $\mathbf{x}_i$. The simplest such representation, which is adequate for our purpose, is to divide $S(t)$ into triangles whose vertices consist of three adjacent $\mathbf{x}_i$'s. These may be chosen to be roughly equilateral at the initial instant, and, provided the distortion of the shape does not become too great (and the collocation points are judiciously chosen), will not become too elongated throughout the evolution. For computational purposes, a list of vertices of each triangle is easy to keep.

At each $\mathbf{x}_i$, the contribution to the integral from any triangle not having a vertex at $\mathbf{x}_i$ may be calculated by the trapezoidal rule (which is tantamount, once the triangle areas are known, to assigning a contribution to each $\mathbf{x}_j, j = 1, \ldots, N$). Unfortunately, however, since $\mathbf{J}$ has a $1/r$ singularity at $r = 0$, the trapezoidal rule is not appropriate for those triangles which do have a vertex at $\mathbf{x}_i$. These must be considered separately, and an analytic representation of the contribution from a 'singular' triangle is given in the appendix. The scheme used to evaluate $\mathbf{u}(\mathbf{x}_i)$ thus consists in running through each collocation point $\mathbf{x}_j, j \neq i$, and adding the trapezoidal rule contribution from each; adding those parts appropriate to the triangles with a vertex at $\mathbf{x}_i$; and finally subtracting again the trapezoidal rule contributions from vertices adjacent to $\mathbf{x}_i$ which would otherwise be counted twice.

3.3. *Choice of the collocation points*

As noted above, for computing the integrals the surface is most appropriately divided into triangles, whereas for computing curvatures five near neighbours are needed for each point. Starting with a unit sphere, the most natural choice for the distribution of collocation points would thus be the vertices of a regular icosahedron, which would provide simultaneously the triangular and pentagonal geometries required. Unfortunately, the side of a icosahedron is (initially) greater than 1 which is too large for acceptable accuracy. Instead, therefore, we use an *ad hoc* mesh of points based on (θ, ϕ) co-ordinates on the sphere surface shown in figure 2.

There are 117 collocation points (those along the dotted line at the bottom are to be identified with the ones at the top), and the surface is thereby divided into 230 triangular regions, none of which has an area greater than 1 % of the total. For three representative points marked 'X' in the diagram, we show circled the five adjacent points used to compute the gradients at X.

3.4. *Numerical stability*

It is straightforward to show on an order-of-magnitude basis that, for stability of the scheme in time, the time step Δt must not be too large. Specifically we require

$$\Delta t \leqslant K \Delta x$$

with K an $O(1)$ constant. In practice, $K = \frac{1}{2}$ was found adequate. Since at the initial instant $\Delta x \approx 0{\cdot}1$, this requires $\Delta t \leqslant 0{\cdot}05$ but when the drop is significantly distorted Δx can be substantially smaller. In fact, for drops of aspect ratio 3 or more, it was found necessary to take $\Delta t \leqslant 0{\cdot}02$, with the unfortunate consequence that the computation time for convergence to equilibrium could be greatly increased.

The criterion that the drop shape had converged to equilibrium was that the normal velocity at each $\mathbf{x}_i$ did not exceed 0·05. If the computation was continued beyond this point, there was very little change in the measured deformation and, by extrapolating the shape at successive times to $t = \infty$ with a Shanks transform, the slow final phase was avoided.

4. Theories for drop deformation

As a preliminary to the presentation of numerical results, we set out in this section the principal theoretical conclusions from asymptotic analyses. It is usual to define a scalar measure of the drop distortion by putting

$$D = \frac{l-b}{l+b}$$

where l, b are the major and minor semi-axes of the drop shape (defined by the largest and smallest distances of the surface from the centre). Then $0 \leqslant D < 1$, $D = 0$ for a sphere, and $D \to 1$ for very high aspect ratio drops. The equilibrium value of D depends upon both Ω and Γ. We denote the critical flow rate for burst (if such exists) by Ω_c and plainly Ω_c is a function of Γ though it is not necessarily uniquely specified by Γ: Hinch & Acrivos (1980) have shown theoretically, and Torza, Cox & Mason (1972)

have demonstrated experimentally, that Ω_c may depend also on the time history of Ω and $\mathbf{\Gamma}$, i.e. how rapidly the shear rate is increased. For the present, however, we consider only time histories in which $\mathbf{\Gamma}$ is constant, and in which Ω is increased very gradually to its final value. We denote by D_c the largest steady sustainable distortion, which occurs at $\Omega = \Omega_c$ if $\Omega_c < \infty$, and is asymptotically attained as $\Omega \to \infty$ if $\Omega_c = \infty$.

As noted in § 1, asymptotic results are available for both large and small drop distortions and are summarized below.

4.1. *Small deformations*

The theory for small deformations has recently been reviewed by Rallison (1980). For weak flows $\Omega \to 0$, the simplest (linear) result due to Taylor (1934) gives an ellipsoidal shape

$$(\mathbf{x}.\mathbf{x})^{\frac{1}{2}} = 1 + \mathbf{x}.\mathbf{A}(t).\mathbf{x},$$

where

$$\frac{\partial \mathbf{A}}{\partial t} = \Omega \mathbf{e} - \frac{64\pi}{35}\mathbf{A}, \tag{5}$$

giving at equilibrium

$$D = \frac{35\Omega}{128\pi}(e_{\max} - e_{\min}), \tag{6}$$

where $e_{\max}$ and $e_{\min}$ are the largest and smallest principal rates of strain. $O(\Omega^2)$ theories involve inclusion of fourth harmonics in the shape, and enable a prediction of Ω_c (Barthès-Biesel & Acrivos 1973). These authors give in particular critical values for simple shear ($\Omega_c = 3{\cdot}9$) and hyperbolic flow ($\Omega_c = 1{\cdot}2$).

In deriving (5) it is assumed that $\boldsymbol{\omega}$ and $\mathbf{e}$ have the same order of magnitude, but if $\|\boldsymbol{\omega}\|/\|\mathbf{e}\| = O(\Omega^{-1}) \gg 1$ then (5) should be replaced by

$$\frac{\mathscr{D}\mathbf{A}}{\mathscr{D}t} = \Omega \mathbf{e} - \frac{64\pi}{35}\mathbf{A}. \tag{7}$$

The appearance of a Jaumann derivative $\mathscr{D}/\mathscr{D}t$ remedies the absence of $\boldsymbol{\omega}$ in (5), and the replacement of $\partial/\partial t$ by $\mathscr{D}/\mathscr{D}t$ occurs also at $O(\Omega^2)$ for general λ, and for $\lambda \to \infty$ for general Ω (Rallison 1980). The equilibrium solution of (7) satisfies

$$\left.\begin{aligned} \Omega(\mathbf{A}.\boldsymbol{\omega} - \boldsymbol{\omega}.\mathbf{A}) + \frac{64\pi}{35}\mathbf{A} &= \Omega\mathbf{e} \\ \text{with} \qquad D &= \tfrac{1}{2}(A_{\max} - A_{\min}). \end{aligned}\right\} \tag{8}$$

For instance, in considering the almost pure rotation flow of § 5.2(*b*) with

$$\mathbf{\Gamma} = \begin{pmatrix} 0 & 1 & 0 \\ \chi & 0 & 0 \\ 0 & 0 & 0 \end{pmatrix} \quad \text{and} \quad \chi \to -1$$

we find

$$D = \tfrac{1}{2}(1+\chi)\,\Omega'/[1 + \Omega'^2(1-\chi)^2]^{\frac{1}{2}}, \quad \text{where} \quad \Omega' = 35\Omega/64\pi, \tag{9}$$

giving

$$\Omega_c = \infty \quad \text{and} \quad D_c \sim \frac{1}{2}\frac{1+\chi}{1-\chi} \quad \text{as} \quad \chi \to -1. \tag{10}$$

Authors	Flow	$\Omega_c(\lambda)$, $\lambda \to 0$
Taylor (1964) Acrivos & Lo (1978)	Uniaxial extension (11)	$0{\cdot}930\lambda^{-\frac{1}{2}}$
Hinch & Acrivos (1979)	Plane hyperbolic (13)	$1{\cdot}82\lambda^{-\frac{1}{2}}$
Hinch & Acrivos (1980)	Simple shear (12)	$0{\cdot}680\lambda^{-\frac{2}{3}}$

TABLE 1. Critical values of Ω for special flows: $\lambda \to 0$.

The time-dependent shape evolution equation (5) indicates a monotonic approach to equilibrium on the surface tension time scale (which is $O(1)$ in our units). When the vorticity terms are important as in (7) on the other hand, there is an oscillatory approach to equilibrium with, at large values of Ω, a spin about the equilibrium on the much shorter shear time scale.

4.2. *Large deformations*

Equations (5) and (7) apply exactly whenever the flow is sufficiently weak or the vorticity sufficiently strong. A more speculative use of existing theory for the $\lambda = 1$ problem concerns the possible applicability of *large* distortion analyses, based on slender-body theory, and developed specifically to consider bubbles of very low viscosity ($\lambda \to 0$). The results obtained for Ω_c in various special flows are shown in table 1.

These analyses have provided also a physical understanding of the dynamics of long thin drops. For example the burst mechanism is shown to be the absence of a sufficiently large pressure gradient inside the drop to push the fluid drawn along the surface toward the tip by the outer flow back along the centre-line. In discussing simple shear, Hinch & Acrivos (1980) show further that the equilibrium shape for flows close to critical can be attained only by very gradual increase of Ω, and that, if Ω is increased too rapidly, then the drop will break. In addition the drop tip is found to approach equilibrium by a spiral.

It is clear that the results for $\lambda = 1$ cannot be expected to conform accurately to either the $\lambda = 0$ or $\lambda = \infty$ theories. We show later that the qualitative physical features shown by these theories do occur for $\lambda = 1$, though the quantitative discrepancies may be quite large.

5. Numerical results

The set of possible shear flows that may be investigated is large in view of the number of choices for the traceless second-rank tensor $\Omega\boldsymbol{\Gamma}$. Since an overall rotation of axes cannot affect the magnitude of drop distortion, nor the critical shear rate for break-up, an exhaustive analysis would require the investigation of a five-parameter space (corresponding, say, to two principal rates of stretching in $\Omega\mathbf{e}$, and the relative orientation and magnitude of the vorticity). Such a task would be enormous, and here we consider instead a range of flows which are experimentally feasible, and which should be representative of the important physics of the drop deformation problem.

5.1. *Uniaxial extensional flow*

This flow is defined by

$$\mathbf{\Gamma} = \begin{pmatrix} 2 & 0 & 0 \\ 0 & -1 & 0 \\ 0 & 0 & -1 \end{pmatrix} \tag{11}$$

so that it is axisymmetric (about the 1-direction), and, starting from a spherical initial condition, the drop shape will remain axisymmetric throughout its time evolution.

This case is discussed for general drop viscosity ratios λ in I, where the azimuthal integrations are performed analytically. By way of a check on the numerical scheme here, the results of I were reproduced and the critical value of Ω ($= 0{\cdot}76$) obtained, to within an acceptable accuracy (3 %). We note in passing that for this flow the magnitude of D is given even at Ω_c to within 20 % by the linear theory (6) but that the $O(\Omega^2)$ theory of Barthès-Biesel & Acrivos (1973) overestimates the magnitude of the distortion for large Ω. The value of Ω_c, on the other hand, is bracketed to within 20 % by the quadratic theory (an underestimate) and the slender-body theory at $\lambda = 1$ (see table 1).

5.2. *Two-dimensional flows*

The class of two-dimensional shear flows, with vorticity in the 3-direction, and principal stretches in the (1, 2)-plane, is defined by the two-parameter family (Ω, χ) where

$$\mathbf{\Gamma} = \begin{pmatrix} 0 & 1 & 0 \\ \chi & 0 & 0 \\ 0 & 0 & 0 \end{pmatrix} \quad \text{so that} \quad \mathbf{e} = \tfrac{1}{2}(1+\chi)\begin{pmatrix} 0 & 1 & 0 \\ 1 & 0 & 0 \\ 0 & 0 & 0 \end{pmatrix} \quad \text{and} \quad \boldsymbol{\omega} = \tfrac{1}{2}(1-\chi)\begin{pmatrix} 0 & 1 & 0 \\ -1 & 0 & 0 \\ 0 & 0 & 0 \end{pmatrix}.$$

Noting that the transformation $(\Omega, \chi) \mapsto (\Omega/\chi, 1/\chi)$ leaves the flow unchanged (by interchange of the 1- and 2-directions), it is clear that without loss of generality χ may be restricted to the range $[-1, 1]$: $\chi = -1$ corresponds to pure rotation; $\chi = 0$ to simple shear; and $\chi = 1$ to plane hyperbolic flow. Thus χ increases with the amount of stretching in $\mathbf{\Gamma}$.

(*a*) *Simple shear flow*, $\chi = 0$:

$$\mathbf{\Gamma} = \begin{pmatrix} 0 & 1 & 0 \\ 0 & 0 & 0 \\ 0 & 0 & 0 \end{pmatrix}. \tag{12}$$

This is the easiest steady shear to reproduce experimentally, and by far the majority of data have concerned this flow. In figure 3 we show a succession of equilibrium drop shapes for increasing flow strengths Ω. For $\Omega \leqslant 2$, the shape perturbation is ellipsoidal to a good approximation, but for larger Ω higher harmonics appear, and for the largest value shown ($\Omega = 5{\cdot}3$) the mid cross-section has an aspect ratio of 3 and is perhaps more accurately pictured as an S-shaped slender body as in Hinch & Acrivos' (1980) analysis for $\lambda \to 0$ than as a near-sphere.

Each equilibrium was obtained by taking as an initial condition for each value of Ω the equilibrium shape attained for a lower value. For $\Omega \lesssim 3$, the new equilibrium was reached after a time $t \approx 0{\cdot}3$, and convergence to the limiting shape was monotonic. For larger Ω, even for small increments, the equilibrium was attained slowly

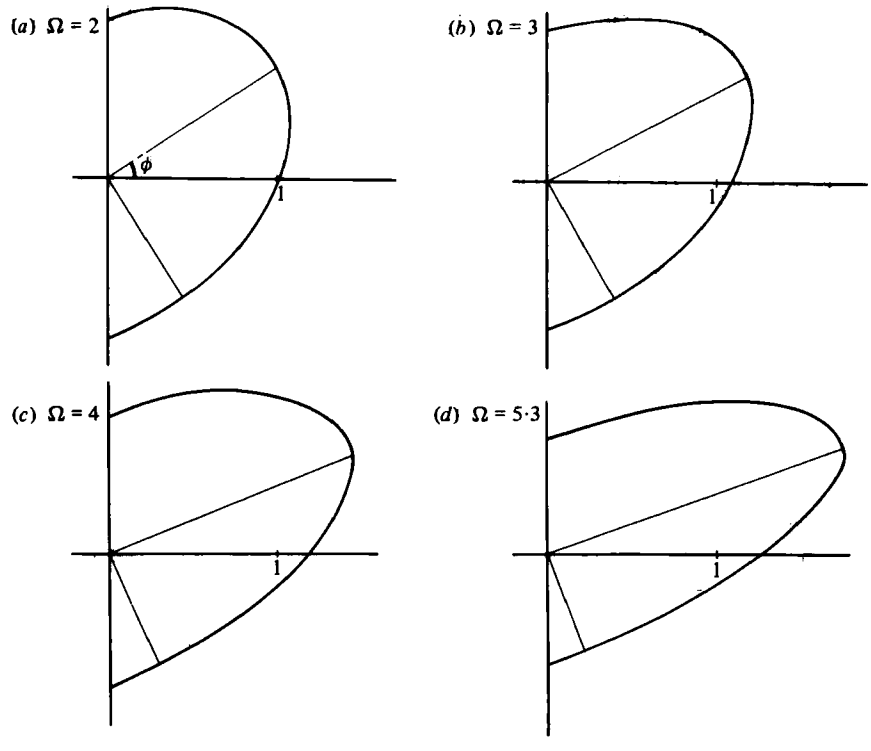

FIGURE 3. Equilibrium shapes for simple shear flow.

($t \approx 1$) and there was a small oscillation of the shape before the equilibrium was obtained. For these highly deformed states it was necessary to take very small time steps ($\Delta t \approx 0{\cdot}01$); otherwise numerical instabilities on the scale of the collocation point spacing appeared.

In figure 4 we summarize the equilibrium results in terms of D and ϕ, the angle between the drop axis and the undisturbed streamlines. It may be seen that the linear theory (6) for D gives extraordinarily good agreement for almost all $\Omega \leqslant \Omega_c$. This must be regarded as fortuitous, since the corresponding result for ϕ ($= 45°$ for all Ω) is poor, and indeed the linear theory for another measure of the deformation (the aspect ratio, say), would involve 30 % errors at $\Omega = 5$. The $O(\Omega^2)$ theory of Barthès-Biesel & Acrivos (1973) is also shown, and, while the deviation *above* the linear theory is qualitatively correct, the quantitative comparison is poor. The effect of including vorticity as in (8) is also to worsen the agreement.

The prediction $\Omega_c = 5{\cdot}3$ compares well with the data of Rumscheidt & Mason (1961); the result given by the quadratic theory is $\Omega_c = 3{\cdot}9$, while the slender body result of table 1 is an underestimate by an order of magnitude.

We now turn to the case where no equilibrium is found for the shape. This always occurs for $\Omega > \Omega_c = 5{\cdot}3$, and may also occur for $\Omega < \Omega_c$ if the flow is increased with sufficient suddenness. Thus Ω_c is a functional over the history of Ω, or, for fixed Ω, of the initial condition for the shape. A careful investigation of this dependence is difficult, in part because so many degrees of freedom are available, and also because, for drops of high aspect ratio, small time steps must be taken. No systematic study

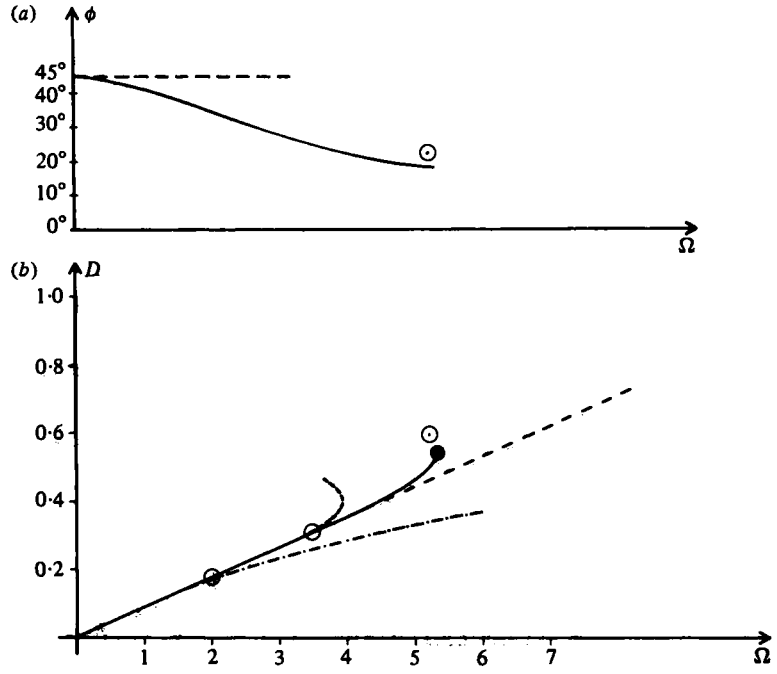

FIGURE 4. Comparison of theories and experiment for simple shear (*a*) the inclination of the drop axis, ϕ; (*b*) the distortion D. ——, numerical results; ●, burst; – – –, linear theory (6); · · · · ·, quadratic theory (Barthès-Biesel & Acrivos (1973)); – · – · – · –, theory with inclusion of vorticity (8); ⊙, experiments of Rumscheidt & Mason (1961).

of this point was undertaken, but it was found that the equilibrium for $\Omega = 5{\cdot}2$ was not attained starting from the converged solution at $\Omega = 4$, but that it was produced starting from that at $\Omega = 5$. This phenomenon was found also for low-viscosity drops by Hinch & Acrivos (1980).

The mode of burst also depended upon the history of Ω. For flow strengths more than about 20 % above Ω_c the drop extended into a long thread aligned closely with the streamlines. With the density of collocation points in this numerical realization, it was possible to follow the time evolution until the drop had an aspect ratio of about 6 (so that the curvature at the ends was in excess of 10). At this point the resolution became inadequate, but the result strongly suggests the type B-2 burst described by Rumscheidt & Mason (1961) with the formation of a long thread which ultimately undergoes a surface-tension instability into a large number of small drops.

A second mode of burst was obtained, though some care was needed to produce it. Rumscheidt & Mason (1961) noted that if Ω was increased to *just* above Ω_c the drop would gradually extend until it had an aspect ratio of about 5, and then suddenly split into two large pieces, with (usually) three small satellite drops between them (type B-1 burst). The difficulty with reproducing this effect numerically is that, since Ω is only just supercritical, a long time is needed for the drop to extend significantly and small time steps must be taken. This process may be speeded up by first increasing Ω to be substantially supercritical and then decreasing it again. Unfortunately, however, this shear history tends to rotate the shape until it is nearly parallel with the

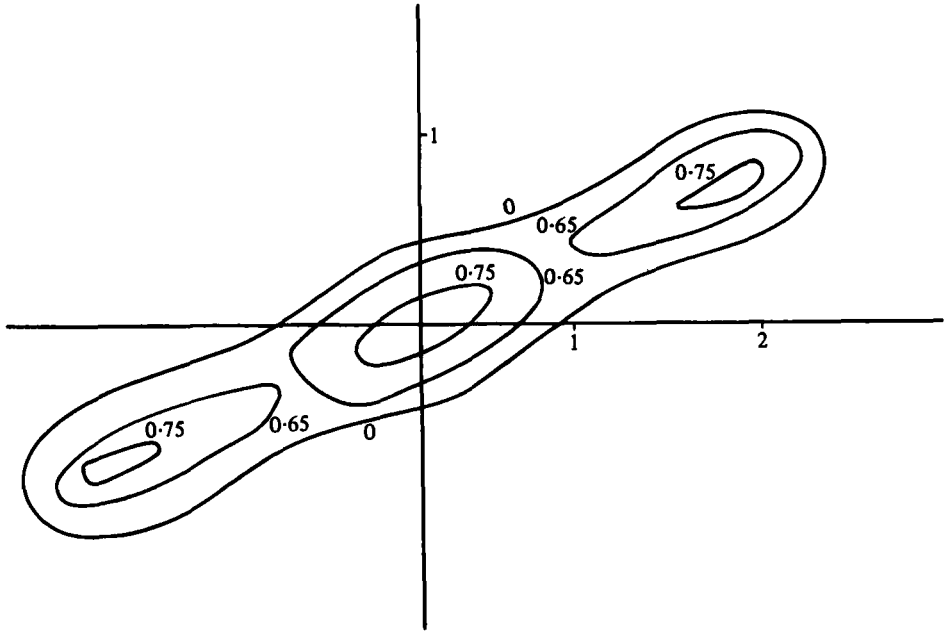

FIGURE 5. Incipient drop break-up (type B-1) in simple shear, contours of constant elevation of drop surface.

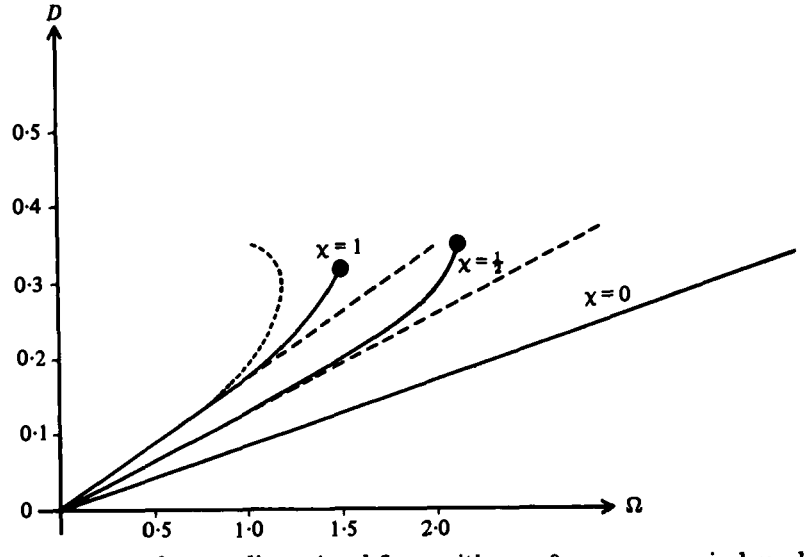

FIGURE 6. Deformation curves for two-dimensional flows with $\chi > 0$. ——, numerical results; ●, burst; – – –, linear theory (6); - - - - -, quadratic theory (Barthès-Biesel & Acrivos (1973)).

streamlines and a type B-2 burst is obtained. An alternative program for $\Gamma(t)$ which did reproduce the desired behaviour, however, was to take

$$\Gamma = \begin{pmatrix} 0 & 1 & 0 \\ 0{\cdot}2 & 0 & 0 \\ 0 & 0 & 0 \end{pmatrix}, \quad \Omega = 6,$$

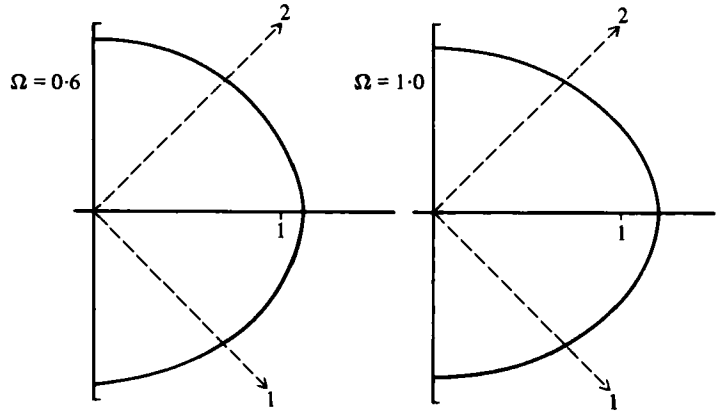

FIGURE 7. Equilibrium drop shapes for hyperbolic flow, $\chi = 1$.

for a time 0·2 following the equilibrium at $\Omega = 5{\cdot}3$ and then to return to simple shear with $\Omega = 6$. The effect of the short burst of the foreign flow is largely to rotate the drop away from the streamlines, and hence subsequently it extends more rapidly. After a further time of order 1, the shape of figure 5 was obtained, in which the lines show contours of constant elevation of the shape. The drop shape is no longer convex, and plainly shows a tendency to break into three pieces. In fact the curvature at certain points of the surface in figure 5 is close to zero and shortly afterwards becomes negative. It proved impossible to follow the bursting process further since it occurs rapidly, with large changes in curvature which, for such a complex shape, are poorly resolved by the hundred or so collocation points. The rapidity of the burst itself agrees with Rumscheidt & Mason's (1961) observation.

(*b*) *Flows with less vorticity than simple shear*, $0 < \chi \leqslant 1$: The class of two-dimensional flows with less vorticity than simple shear is bounded at the opposite extreme by plane hyperbolic flow, $\chi = 1$. With axes as chosen, the principal directions of stretching and compression are at 45° to the 1-direction, but by rotation of axes the more conventional choice

$$\boldsymbol{\Gamma} = \begin{pmatrix} 1 & 0 & 0 \\ 0 & -1 & 0 \\ 0 & 0 & 0 \end{pmatrix} \tag{13}$$

would give the same results for D and Ω_c.

In figure 6 we show the full deformation curves for $\chi = 1$ and 0·5 and part of the result for $\chi = 0$. It is again apparent that the linear theory (6) gives extraordinarily good agreement with the numerical results. The fit is best for $\chi = 0$, but underestimates D by only 10 % at burst even for $\chi = 1$.

For hyperbolic flow, the results are very similar to those for uniaxial extension discussed in § 5.1. Again, inclusion of quadratic terms (Barthès-Biesel & Acrivos 1973) worsens the quantitative accuracy for D but is qualitatively correct (see figure 6) and produces an underestimate for Ω_c by 15 %. The slender body result for Ω_c in table 1 is an overestimate by 20 % which is surprisingly good considering the smallness of D_c. The experiments of Rumscheidt & Mason (1961) show close agreement with the linear theory for D, and a value for Ω_c ($= 1{\cdot}3$) which is very close to the quadratic result, but is lower than that found here (1·5). The corresponding D_c ($= 0{\cdot}5$),

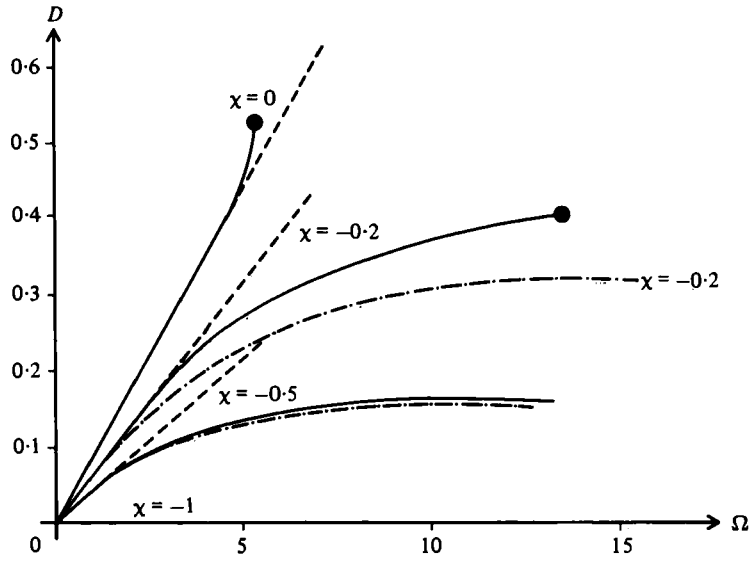

FIGURE 8. Deformation curves for two-dimensional flows with $\chi < 0$. ——, numerical results; ●, burst; – – –, linear theory (6); – · – · – · –, theory with inclusion of vorticity (8).

however, is substantially higher than that predicted by either theory; the reason for this discrepancy is not known.

It is readily apparent, as predicted by all the (nonlinear) theories of drop deformation, that an increase in vorticity (χ decreasing) leads to a decrease in D for given Ω, and an increase in Ω_c. The physical reason, which is easily seen for high-viscosity drops, is that the higher the vorticity the more rapidly the material inside the drop rotates, and so the higher the frequency of oscillation of stretching and compression due to **e** as seen in a frame fixed in the drop, and thus the smaller the distortion. It can also be seen from figure 6 (compare also figures 3 and 7) that, as χ decreases from 1, so the limiting distortion D_c increases. Thus in hyperbolic flow, the largest sustainable steady distortion is considerably smaller than the largest available for simple shear.

(c) *Flows with more vorticity than simple shear*, $-1 \leqslant \chi < 0$: The extreme flow of this class is pure rotation about the 3-direction when $\chi = -1$. In that case it is physically obvious that the drop will rotate without deformation however large Ω may be, and thus

$$D = 0 \quad \text{for all } \Omega, \quad \Omega_c = \infty.$$

In figure 8 we show the deformation curves for $\chi = -0{\cdot}2, -0{\cdot}5$. The curve for $\chi = -0{\cdot}2$ stops at $\Omega = 13$ where the drop bursts, with an oscillatorily growing instability. The growth rate of the instability is small and involves several cycles of oscillation of the entire shape. For $\chi = -0{\cdot}5$, on the other hand, no critical flow rate was found. For values of Ω beyond 10 (up to 25), no significant increase in D could be obtained and apparently $\Omega_c = \infty$ for that case. For each value of $\Omega > 3$, approach to equilibrium was by a spiral.

For flows with such strong vorticity, the linear theory (6) for D was found to have a small range of usefulness (see figure 8), and the numerical results deviated significantly

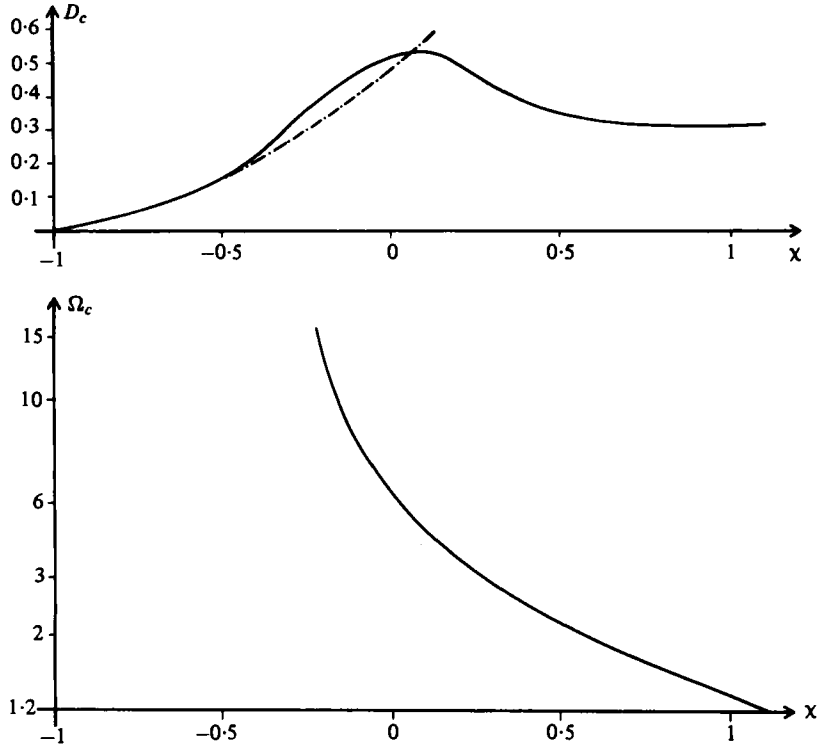

FIGURE 9. Critical values for two-dimensional flows. (*a*) Deformation D_c. (*b*) Flow rate Ω_c. ——, numerical results; – · – · – · –, theory (10) for $\chi \to -1$.

below the linear predictions. The inclusion of the vorticity term as in (8), however, produced much closer agreement, with quite accurate results for $\chi = -0{\cdot}5$.

On the basis of the results for all the two-dimensional flows summarized in figure 9, it is clear that, for $\chi < \chi_c \approx -0{\cdot}3$, no flow rate, however strong, will break the drop. This result is highly reminiscent of the corresponding asymptotic unbreakability in simple shear of drops whose viscosity ratio exceeds 3·4 (Grace 1971): plainly an increase of internal viscosity or of vorticity inhibits and ultimately prevents drop break-up in shear.

In figure 9 we show also the largest sustainable steady deformations $D_c(\chi)$. For $\chi \lesssim \chi_c$ the drop shape approaches a steady small deformation as $\Omega \to \infty$ which is vanishingly small for $\chi = -1$ and, since flows with little vorticity ($\chi \to 1$) are more effective in breaking the drop, D_c has a maximum over χ which is found to occur just beyond simple shear at $\chi \approx 0{\cdot}1$.

5.3. *Orthogonal rheometer flows*

The linear flow generated between two offset rotating disks (an orthogonal rheometer) gives rise to the two-parameter family (Ω, ψ), where

$$\mathbf{\Gamma} = \begin{pmatrix} 0 & 1 & -\psi \\ 0 & 0 & 0 \\ \psi & 0 & 0 \end{pmatrix}$$

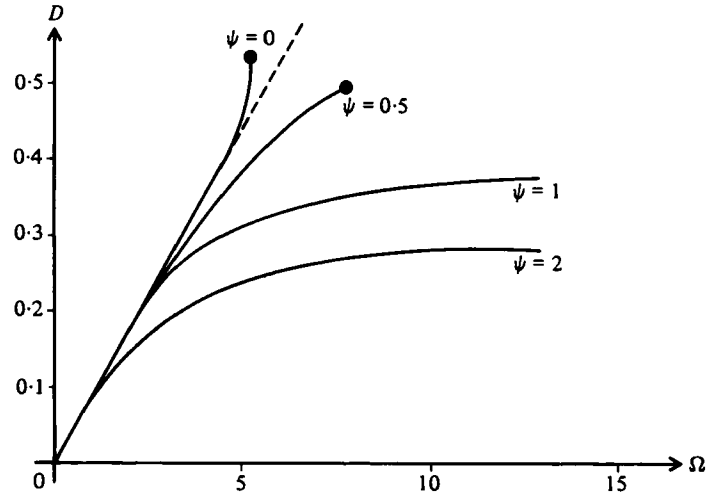

FIGURE 10. Deformation curves for orthogonal rheometer flows. ——, numerical results; ●, burst; – – –, linear theory (6).

so that

$$\mathbf{e} = \frac{1}{2}\begin{pmatrix} 0 & 1 & 0 \\ 1 & 0 & 0 \\ 0 & 0 & 0 \end{pmatrix}$$

and

$$\boldsymbol{\omega} = \frac{1}{2}\begin{pmatrix} 0 & 1 & -2\psi \\ -1 & 0 & 0 \\ 2\psi & 0 & 0 \end{pmatrix} \quad \text{with} \quad \psi > 0.$$

This flow has been used by Hakimi & Schowalter (1980) in an experimental investigation of the deformation of comparatively inviscid drops ($\lambda \approx 0{\cdot}1$), but as yet has not been used for drops with $\lambda = 1$. The limiting case $\psi = 0$ is simple shear in the (1, 2)-plane and has been investigated above, whereas the opposite extreme $\psi = \infty$ is pure rotation about the 2-direction. For all values of ψ, the vorticity in such flows is substantial, greater than that in simple shear, and thus is weak in regard to generating deformation and burst (Schowalter 1979).

The drop shape for such a flow has a complex three-dimensional structure. For small values of ψ ($\approx 0{\cdot}5$) it is found that the largest deformations are, for all values of Ω up to Ω_c, confined close to the (1, 2)-plane. For larger values of ψ, however, at modest Ω, the largest deformations lie in the (1, 2)-plane as the linear theory (6) suggests, but for larger Ω the principal axes lie rather in the (2, 3)-plane and no burst occurs however large Ω.

In figure 10 we show the deformation curves for a representative set of ψ. The linear theory gives $D = 0{\cdot}087\Omega$ as for simple shear for all values of ψ since it takes no account of the vorticity. The inclusion of the Jaumann derivative as in (8) which is formally valid only for $\psi \to \infty$ improves the qualitative agreement and gives $\Omega_c = \infty$, but for $\psi \gtrsim 2$ the quantitative accuracy is poor with D at $\Omega = 4$ for $\psi = 2$ still overestimated by 15 %.

6. Conclusions

We summarize here the principal results of the numerical study.

As regards equilibrium drop shapes, for flows in which the vorticity is not too strong, $\|\boldsymbol{\omega}\| \lesssim \|\mathbf{e}\|$, the deformation measured by D is given to within 10 % over the entire subcritical range of flow strengths by the linear theory (6). The agreement is less good for $\|\boldsymbol{\omega}\| > \|\mathbf{e}\|$, though in that case the inclusion of vorticity (8) gives an improvement, and when $\|\boldsymbol{\omega}\| \geqslant 4\|\mathbf{e}\|$ is quite accurate.

The presence of vorticity is found to inhibit drop deformation and burst significantly, so that for flows with sufficient vorticity the drop will not burst however high the flow rate. Theoretical predictions of Ω_c for extensional flows from both small and large deformation analyses give agreement to within 15 %, the small deformation result an underestimate, and the slender-body theory an overestimate. For shear flows, the large deformation result is inapplicable but the small deformation result still provides agreement to 20 %.

Finally we note that the numerical techniques developed in this paper and in I enable general drop viscosities and arbitrary shear flows to be considered. Our results have been restricted mainly to steady flows, but the method may similarly be applied to general prescribed shear histories.

This work was supported in part by NATO Research Grant no. 1442. I am grateful to Professor A. Acrivos and Dr E. J. Hinch for numerous helpful suggestions.

Appendix. Evaluation of the singular integral over an elemental triangle

In determining the fluid velocity generated by the surface tension forces we need to evaluate integrals of the form

$$I = \int_{\Delta S} \frac{1}{r} g(r)\, dS$$

over the triangle ΔS shown in figure 11.

The points O, X, Z are adjacent collocation points and so the quantity g (which involves curvature and normals at each) is known at the vertices, and is supposed

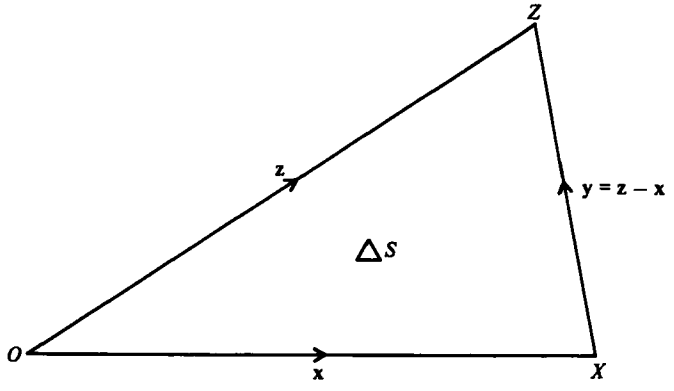

FIGURE 11. Definition sketch for an elemental triangle in the drop surface.

well-behaved throughout ΔS. The vectors $\mathbf{x}, \mathbf{y}, \mathbf{z}$ have magnitudes x, y, z which are small ($O(\Delta x)$) and in consequence the overall area of the triangle

$$\Delta S = \tfrac{1}{2}[x^2 z^2 - (\mathbf{x}.\mathbf{z})^2]^{\frac{1}{2}} = O(\Delta x^2).$$

We may then write for $\mathbf{r} \in \Delta S$,

$$g(\mathbf{r}) = g_O + A\mathbf{x}.\mathbf{r} + B\mathbf{z}.\mathbf{r} + O(\Delta x^2),$$

in which

$$A = [z^2(g_X - g_O) - \mathbf{x}.\mathbf{z}(g_Z - g_O)]/4\Delta S^2$$

and

$$B = [x^2(g_Z - g_O) - \mathbf{x}.\mathbf{z}(g_X - g_O)]/4\Delta S^2,$$

and it is then straightforward to show that

$$I = \frac{2\Delta S}{y}\left\{\left[g_O + \frac{2\Delta S^2}{y^2}(A+B)\right]\ln\frac{x+y+z}{x-y+z} + \tfrac{1}{4}[(B-A)\,y(z-x) + (B+A)\,(z-x)^2(z+x)/y]\right\} + O(\Delta x^3).$$

REFERENCES

Acrivos, A. & Lo, T. S. 1978 Deformation and breakup of a single slender drop in an extensional flow. *J. Fluid Mech.* **86**, 641.

Barthès-Biesel, D. & Acrivos, A. 1973 Deformation and burst of a liquid droplet freely suspended in a linear shear field. *J. Fluid Mech.* **61**, 1.

Grace, H. P. 1971 Dispersion phenomena in high viscosity immiscible fluid systems and applications of static mixers as dispersion devices in such systems. *Engng Found. 3rd Res. Conf. Mixing, Andover, New Hampshire.*

Hakimi, F. S. & Schowalter, W. R. 1980 The effects of shear and vorticity on deformation of a drop. *J. Fluid Mech.* **98**, 635.

Hinch, E. J. & Acrivos, A. 1979 Steady long slender droplets in two-dimensional straining motion. *J. Fluid Mech.* **91**, 401.

Hinch, E. J. & Acrivos, A. 1980 Long slender drops in a simple shear flow. *J. Fluid Mech.* **98**, 305.

Rallison, J. M. 1980 Note on the time-dependent deformation of a viscous drop which is almost spherical. *J. Fluid Mech.* **98**, 625.

Rallison, J. M. & Acrivos, A. 1978 A numerical study of the deformation and burst of a viscous drop in an extensional flow. *J. Fluid Mech.* **89**, 191.

Rumscheidt, F. D. & Mason, S. G. 1961 Particle motions in sheared suspensions. XII. Deformation and burst of fluid drops in shear and hyperbolic flows. *J. Colloid Sci.* **16**, 238.

Schowalter, W. R. 1979 Some consequences of suspension models for non-viscometric flows. *J. Non-Newtonian Fluid Mech.* **5**, 285.

Taylor, G. I. 1934 The formation of emulsions in definable fields of flow. *Proc. Roy. Soc.* A **146**, 501.

Taylor, G. I. 1964 Conical free surfaces and fluid interfaces. *Proc. 11th Int. Cong. Appl. Mech., Munich.*

Torza, S., Cox, R. G. & Mason, S. G. 1972 Particle motions in sheared suspensions. XXVII. Transient and steady deformation and burst of liquid drops. *J. Colloid Interface Sci.* **38**, 395.